IAEA-CN-37/L-4

CONF-780811--21

EXPERIMENTAL AND THEORETICAL STUDIES OF THE ELMO BUMPY TORUS (EBT)*

R.A. Dandl, F.W. Baity, Jr., K.H. Carpenter, J.A. Cobble, H.O. Eason, J.C. Glowienka, G.R. Haste, M.E. Hesse,† S. Hiroe, N.H. Lazar, B.H. Quon, T. Uckan, T.L. White, Heavy Ion Beam Group,‡ and UV Spectroscopy Group§
Oak Ridge National Laboratory, Oak Ridge, Tennessee 37830 U.S.A.

and

C.L. Hedrick, D.B. Batchelor, L. Deleano, R.C. Goldfinger, E.F. Jaeger, L.W. Owen, D.A. Spong, and J.S. Tolliver
Oak Ridge National Laboratory, Oak Ridge, Tennessee 37830 U.S.A.

and

J.B. McBride, N.A. Krall, and A.L. Sulton, Jr.
Science Applications, Incorporated, La Jolla, California 92037 U.S.A.

ABSTRACT

The confinement of plasma produced by electron cyclotron heating in the ELMO Bumpy Torus (EBT) has been studied in the regime stabilized by the diamagnetism of annular, energetic electrons. The electron density (n_e = 1-2 x 10^{12} cm^{-3}) and temperature ($150 \leq T_e \leq 600$ eV) and ion temperature ($30 \leq T_i \leq 150$ eV) have been measured over a range of operating conditions. Measurement of the direction of the electric field (inward pointing) inside the toroidally confined plasma has led to improved neoclassical theoretical models of plasma transport which describe reasonably well the observed parameter dependences over a wider range of collisionality than reported previously.

---

*Research performed under Union Carbide Corporation Contract W-7405-eng-26 with the Office of Fusion Energy (ETM), U. S. Department of Energy.

†On leave from Centre d'Etudes Nucleaires de Grenoble, Grenoble, France

‡F.M. Bieniosek, F.J. Bresnock, P.L. Colestock, K.A. Connor, R.L. Hickok, and S.S. Kuo, Rensselaer Polytechnic Institute, Troy, New York

§H.W. Moos, J.M. Tyson, and E.S. Warden, The Johns Hopkins University, Baltimore, Maryland

---

I. EXPERIMENTAL STUDIES

The plasma in the ELMO Bumpy Torus (EBT) [1] is confined in steady state in a "bumpy" magnetic field produced by joining 24 magnetic mirror cells into a large aspect ratio torus. Heating power is provided by cw microwaves resonant at electron cyclotron frequencies at both 18 GHz (up to 60 kW) and 10.6 GHz (up to 30 kW); the latter is used primarily to sustain the energetic electron population and form the diamagnetic annuli.

The toroidal plasma in EBT has been shown to be macroscopically stabilized by the field modification resulting from the diamagnetic electron annuli [1]. The plasma properties have been measured over a sufficient range of operating parameters – in this stabilized magnetic configuration, using a broad spectrum of diagnostic techniques – that general correlations with neoclassical theoretical models can now be made. This close interplay between experiment and theory has led to improvements in the models and better understanding of the plasma which has intensified the incentive to raise the applied microwave frequency, heating power, and toroidal magnetic field.

In the macrostable regime, free-free bremsstrahlung measurements have been obtained to determine the toroidally confined electron temperature and density. The temperatures are observed to rise with decreasing ambient pressure or increased power and lie in the range $150 \leq T_e \leq 600$ eV. The observed densities follow, in general, a similar behavior and increase by about a factor of three to a maximum of $n_e \sim 2 \times 10^{12}$ cm^{-3} in this operating range. These data may be combined with applied power to evaluate the energy lifetime of the toroidal plasma component. Assuming that the fraction of applied power deposited in the toroidal component (compared to the power to sustain the energetic annulus and the surface plasma) is constant, in Fig. 1 we present the energy lifetime (normalized by multiplying by electron temperature) plotted against the electron collisionality $\nu/\Omega = 2.7 \times 10^{-7}\, n/T_e^{5/2}\, [1 + (0.7)e\phi/T_e]^{-1}$. Also shown are curves calculated from neoclassical transport rates which take into account the ambipolar electric field. In this same range, the charge-exchange neutral energy distribution has been measured using both nitrogen and cesium charge-exchange cells with $30 \leq T_i \leq 150$ eV. The radial distribution of the ion temperature has also been determined from an array of four spatial channels. The energetic plasma ions lie within the diamagnetic annuli, r = 15 cm. An energetic Rb^+ beam has been injected through the plasma and the plasma potential determined from measurements of the change in beam energy of multiply charged rubidium ions which results from ionization in the bulk electron population [2]. Spatial mapping of the points of ionization confirms the plasma size described above and provides a direct measurement of the ambipolar electric field. The potential at the center of the plasma lies in the range -100 to +100 V and is negative relative to the potential maximum found at the position of the annulus. The relatively good agreement in shape of the points in Fig. 1 with the curve for $e\phi/T_e = 1$ is especially significant since the measured potentials are consistent with this value.

Optimization of the plasma parameters occurs when magnetic error fields are globally canceled by superimposed, weak, quadrupole magnetic fields. With this optimization, toroidal plasma currents (normally ~100 A), which are driven by the component of the ambipolar electric field along the magnetic field lines, are nulled, fluctuation levels are minimized, and almost complete symmetry of the radial electric field is measured. An example of these data is shown in Fig. 2 as a function of the imposed horizontal error field produced by one pair of the quadrupole winding.

Spatially resolved spectroscopic impurity measurements have been carried out using stereoscopic observation of the emitted u.v. and visible characteristic line radiation. The impurities (primarily carbon and sputtered aluminum) are found predominantly in the space outside the region of closed drift surfaces filled by the hot, bulk plasma. In the toroidal plasma region,

$\frac{n\ (carbon)}{n_e} = 6 \times 10^{-5}$, whereas in the surface plasma outside this region,

$\frac{n\ (carbon)}{n_e} \sim 10^{-2}$. Aluminum densities are the same order of magnitude.

In order to permit observations over an expanded plasma parameter range, a 28-GHz, 200-kW, cw, gyrotron [3] is under development for EBT use by Varian Associates. Theoretical results indicate increased densities and temperatures can be expected from the higher power, shorter wavelength heating sources. Experiments are presently under way at these higher magnetic fields, and initial results will be described.

II. EBT THEORETICAL STUDIES FOCUSING ON TRANSPORT

Here we discuss the latest neoclassical transport description of EBT losses which has been sufficiently refined to self-consistently include the ambipolar electric field. Other theoretical topics are discussed by N. A. Uckan et al. [4].

Transport rates in EBT depend sensitively on the radial ambipolar electric field in contrast to other devices, such as tokamaks [5-7]. In the absence of such a field, electrons and ions of the same energy and pitch angle have coincident orbits and step sizes; electron particle fluxes would thus greatly exceed those of ions due to their higher collision frequency. The resulting ambipolar electric field equalizes the electron and ion particle fluxes and greatly influences plasma confinement.

There are two simply conceptualized ways of producing equality of the two fluxes. First, a radially outward pointing field can electrostatically confine electrons, reducing their flux to that of the ions. Alternately, a radially inward pointing electric field (for normal magnetic gradient regions) will enhance ion diffusion by a cancellation of the $\vec{E} \times \vec{B}$ poloidal drift with the magnetic poloidal drifts. The latter mechanism is apparently relevant to the stable T-mode of EBT-I. Indeed, the experimentally observed sign of the electric field changes sign near the minor radius at which the gradient in B is reversed by the hot electron annuli — as required for partial cancellation of the ion magnetic and $\vec{E} \times \vec{B}$ drift to produce banana shaped orbits.

The ORNL one-dimensional radial transport model, which has been developed to simulate the T-mode of operation self-consistently, calculates the ambipolar potential and temperature profiles [7]. Figures 3 and 4 show typical results of these calculations. From Fig. 3 it is apparent that there are three roots to the particle flux condition $\Gamma_i = \Gamma_e$. The positive root corresponds to the electrostatic mechanism mentioned earlier. The two roots near the peak in Γ_i correspond to the mechanism which involves partial cancellation of $\vec{E} \times \vec{B}$ and magnetic drift motion. As described in Ref. [7], only the most negative electric field value of $\Gamma_i = \Gamma_e$ in Fig. 3 provides thermally stable solutions. The stability of this type of solution is relatively insensitive to boundary conditions. For example, the neutral edge density may be treated as a constant or reflux boundary conditions may be used.

The results obtained using this model give lower temperatures or higher collisionality than experimental observations indicate. In fact, calculations of Ref. [7] are based on transport coefficients whose validity is limited to high collisionality. At lower collisionality, the details of particle orbits (e.g., banana shaped orbits) become more important. Recently, we have developed a formalism for calculating EBT neoclassical transport coefficients which allows inclusion of such orbit details. While the preliminary results are extremely encouraging, the full import of these newer transport coefficients remains to be assessed.

III. SPACE-AVERAGED EBT MODELING

Although multidimensional models, as discussed in the previous section, contain a wealth of detail, space-averaged ("point") models are also useful, both in obtaining scans of parameter space for scaling studies and in identifying equilibria which can be the starting point for 1-D studies. In this section, we present such a model and demonstrate its ability to produce results comparable to the 1-D treatment. The model equations assume neoclassical losses as in the previous section, replacing gradient scale lengths by the plasma minor radius. The model equations are those given in Refs. [6,8], except that we now distinguish the neoclassical particle confinement time τ_p from the electron and ion energy confinement times τ_{Ee} and τ_{Ei} [5].

$$\tau_{p\alpha}^{-1} = \frac{4}{3}\left(\frac{R_c}{R_T}\right)^2 \nu_\alpha \frac{\left(1 + 2\eta_\alpha + q_\alpha L_n E/T_\alpha\right)}{\left(1 + q_\alpha E R_c/T_\alpha\right)^2 + \nu_\alpha^2/\Omega_{0\alpha}^2}$$

$$\frac{\tau_p}{\tau_{E\alpha}} = \frac{7}{2} \frac{\left(1 + 101/7\ \eta_\alpha + q_\alpha L_n E/T_\alpha\right)}{\left(1 + 2\eta_\alpha + q_\alpha L_n E/T_\alpha\right)}$$

Ambipolarity constrains $\tau_{pe} = \tau_{pi} = \tau_p$ and thus determines the self-consistent radial electric field. η_e and η_i are the ratios of density gradient scale length to the electron and ion temperature gradient scale lengths, typically chosen to be unity. The neutral density is related to the plasma density by $n_0 + \varepsilon n$ = constant. The model is flexible in that the total particle density, plasma plus neutrals, can be held fixed by choosing $\varepsilon = 1$, while the neutral density is fixed if we choose $\varepsilon = 0$. The form of this relation has no effect on the operating equilibria but influences the stability.

Figure 5 shows typical power balance curves for EBT-I, illustrating the scaling trends predicted by the point model. We chose the input parameters to characterize EBT-I, assuming that the microwave power absorbed is $P_\mu = 10^4$ W/M^3. Note the existence of negative electric field solutions at the higher densities, where the electrons and ions are apparently well coupled thermally. As the density decreases, the negative electric field branch gives way to a positive electric field branch along which the temperature rises and the plasma becomes highly collisionless. The negative electric field branch is characterized by collisional scaling and the confinement is controlled by the ions $\tau \sim \tau_{Ei}$. When the field changes sign at lower density and lower collisionality, the confinement becomes controlled by the electrons $\tau \sim \tau_{Ee}$. The positive electric field branch exhibits both stable and unstable operating points regardless of the neutral model. The highly collisionless (dotted) portion is always unstable, while the lower temperature (solid) portion is always stable. The stability of

the negative electric field branch (dashed) is much more sensitive to the neutral model. The model used here predicts stable operation along the negative field branch, as in the experiment, for $\varepsilon \gtrsim 10 n_0/n \gtrsim 10^{-2} - 10^{-1}$. Thus, the stability of the negative roots is sensitive to the feedback stabilizing influence of the neutral particles. The scaling trends, sign of the ambipolar fields, and stability properties of the various branches in Fig. 5 are consistent with the 1-D code calculations.

As in 1-D, we find that higher power tends to shift the operating characteristics to higher density and somewhat higher temperature while not substantially altering the shape of the curves. In all cases, however, temperatures were somewhat lower on the negative field branch (perhaps a factor of 2-4) than the highest temperatures reported by the experimenters.

We conclude that neoclassical operation on the collisional negative electric field branch is roughly consistent with the lower temperature regimes measured in EBT, but not with the higher temperature collisionless regimes also observed experimentally (which correspond to negative ambipolar electric fields). Additional physics input to the model is thus required if in fact a neoclassical description of plasma loss is adequate for the collisionless regime.

REFERENCES

[1] DANDL, R.A., EASON, H.O., EDMONDS, P.H., ENGLAND, A.C., GUEST, G.E., HEDRICK, C.L., HOGAN, J.T., SPROTT, J.C., in Plasma Physics and Controlled Nuclear Fusion Research (Proc. Conf. Madison, WI, 1971), Vol. II, IAEA, Vienna (1971) 607; DANDL, R.A., EASON, H.O., GUEST, G.E., HEDRICK, C.L., IKEGAMI, H., NELSON, D.B., in Plasma Physics and Controlled Nuclear Fusion Research (Proc. Conf. Tokyo, Japan, 1974), Vol. II, IAEA, Vienna (1975) 141.

[2] COLESTOCK, P.L., CONNOR, K.A., HICKOK, R.L., and DANDL, R.A., Phys Rev. Lett. 40 (1978) 1717.

[3] ZAYTSEV, N.I., PANKRATOVA, T.B., PETELIN, M.I., FLYAGIN, V.A., "Millimeter- and Submillimeter-Wave Gyrotrons," Radiotekh. Electron. [Radio Eng. Electron. Phys.] 19 (1974) 1056-60.

[4] UCKAN, N.A., et al., "The ELMO Bumpy Torus (EBT) Reactor," Paper I-3, this meeting.

[5] KOVRIZNYKH, L.M., Sov. Phys. – JETP 29 (1969) 475.

[6] HEDRICK, C.L., et al., Nucl. Fusion 17 (1977) 1237.

[7] JAEGER, E.F., et al., Phys. Rev. Lett. 40 (1978) 866.

[8] McBRIDE, J.B., and SULTON, A.L., Jr., Nucl. Fusion 18 (1978) 285.

FIGURE CAPTIONS

FIG. 1. Product of electron temperature, T_e, and energy confinement time, $\tau_E = \int \frac{nT_e dV}{P}$, as a function of electron collisionality. Data points were obtained from bremsstrahlung measurements over a wide range of operating power and ambient neutral density.

FIG. 2. Influence of horizontal component of imposed error field on various plasma parameters: Plasma potential well (potential difference between potential maximum and minimum), plasma density fluctuations seen on 70-GHz interferometer, plasma density ($n_e \ell$), and toroidal current measured with pickup loop.

FIG. 3. Electron and ion particle flux versus ambipolar electric field.

FIG. 4. Steady-state radial profiles of plasma density, n, ambipolar potential, ϕ, electron temperature, kT_e, and ion temperature, kT_i.

FIG. 5. Operating characteristics for EBT-I.

ORNL/DWG/FED 78–393

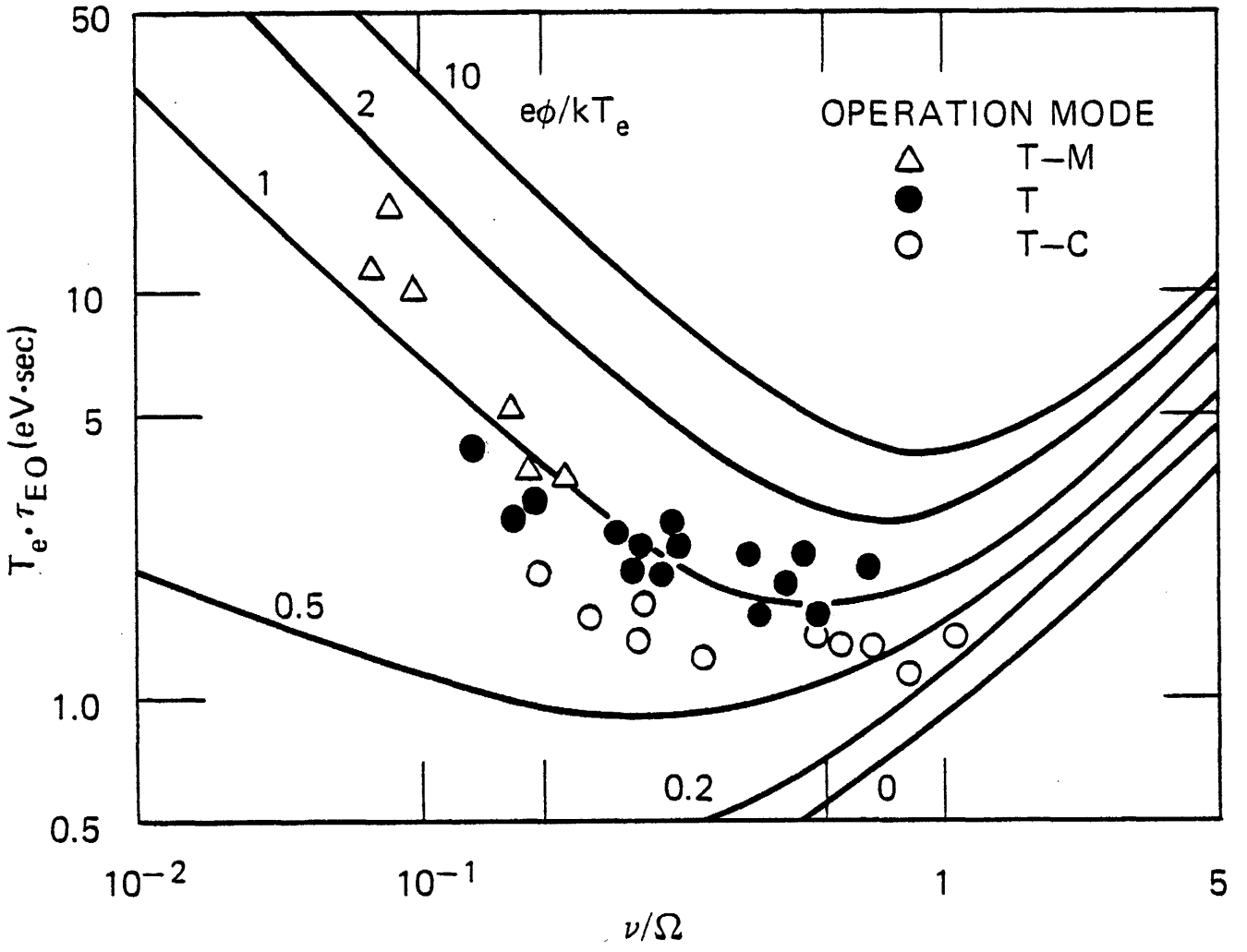

FIG. 1. Product of electron temperature, T_e, and energy confinement time, $\tau_E = \int \frac{nT_e dV}{P}$, as a function of electron collisionality. Data points were obtained from bremsstrahlung measurements over a wide range of operating power and ambient neutral density.

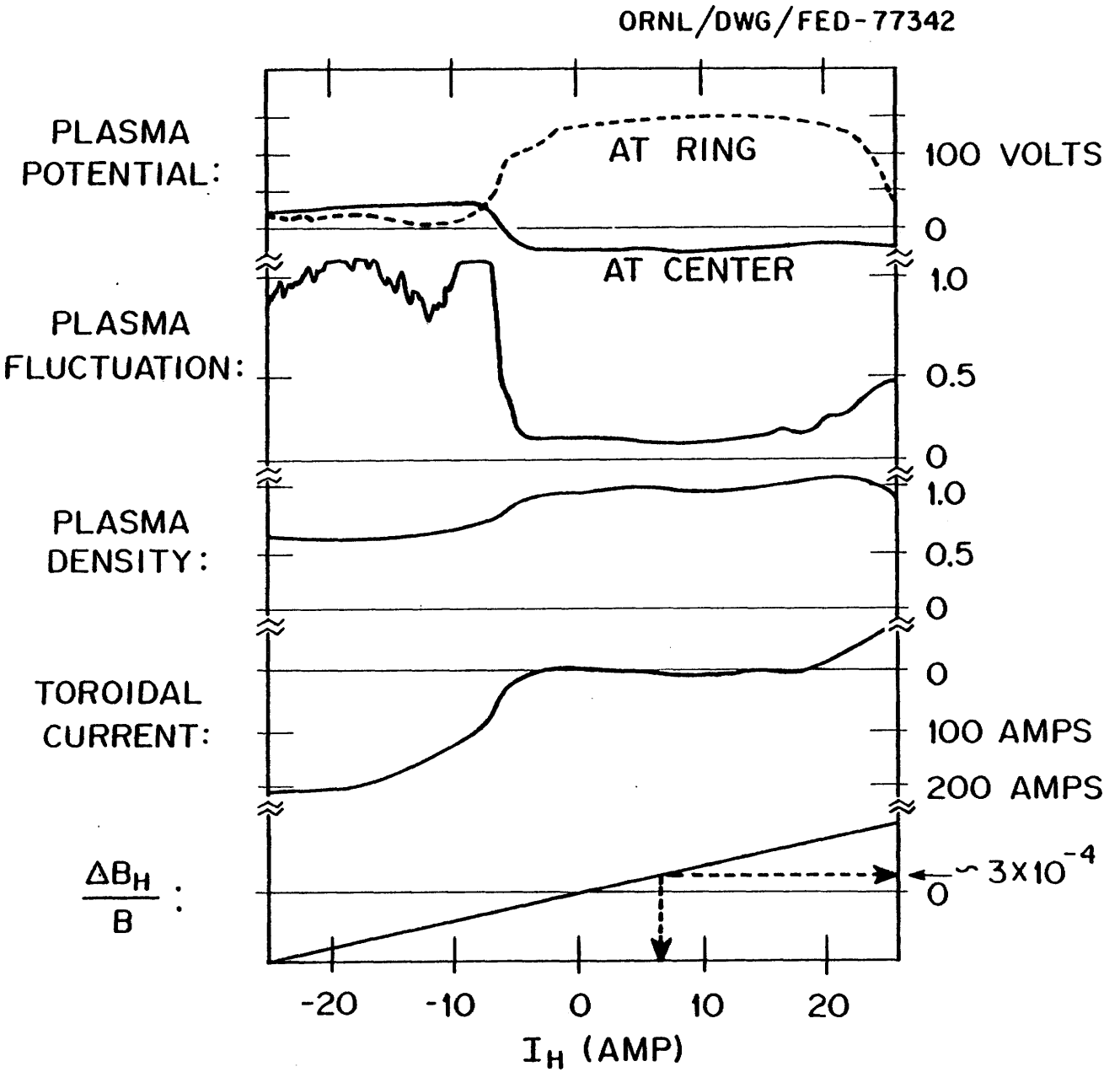

FIG. 2. Influence of horizontal component of imposed error field on various plasma parameters: Plasma potential well (potential difference between potential maximum and minimum), plasma density fluctuations seen on 70-GHz interferometer, plasma density ($n_o \ell$), and toroidal current measured with pickup loop.

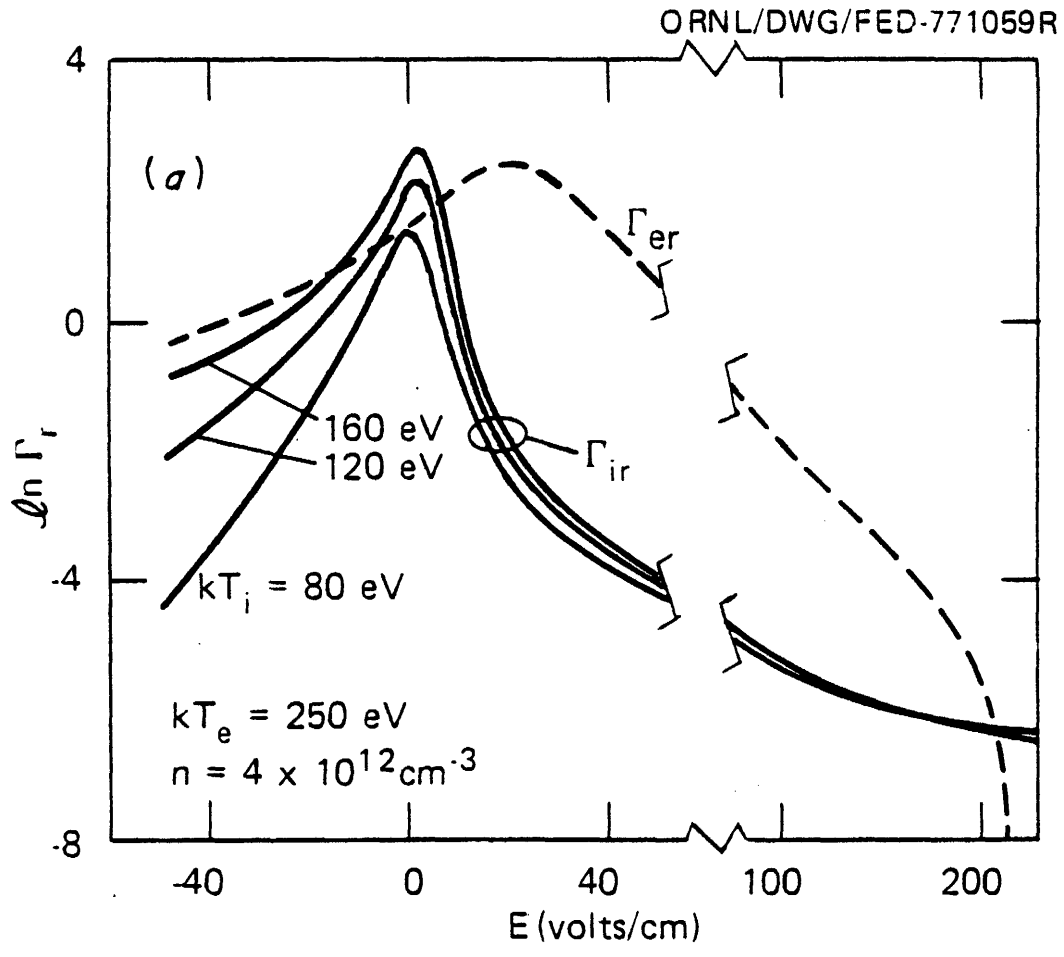

FIG. 3. Electron and ion particle flux versus ambipolar electric field.

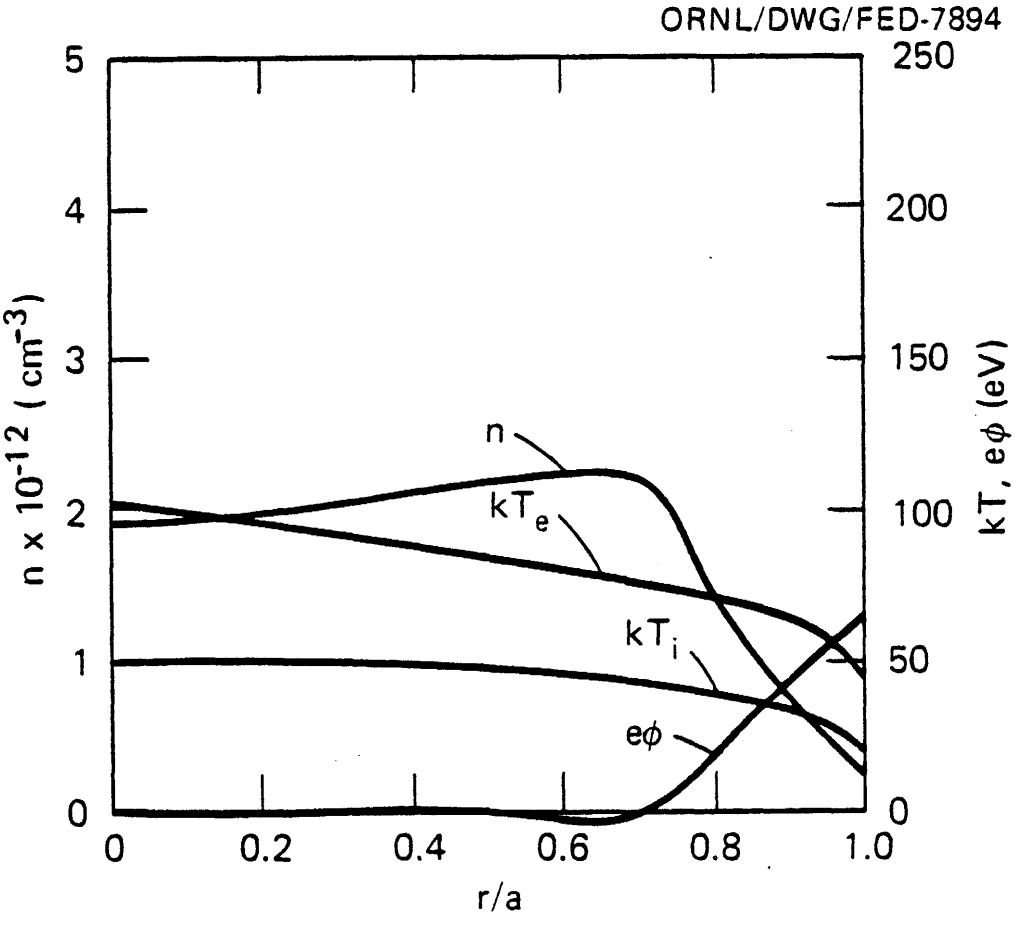

FIG. 4. Steady-state radial profiles of plasma density, n, ambipolar potential, ϕ, electron temperature, kT_e, and ion temperature, kT_i.

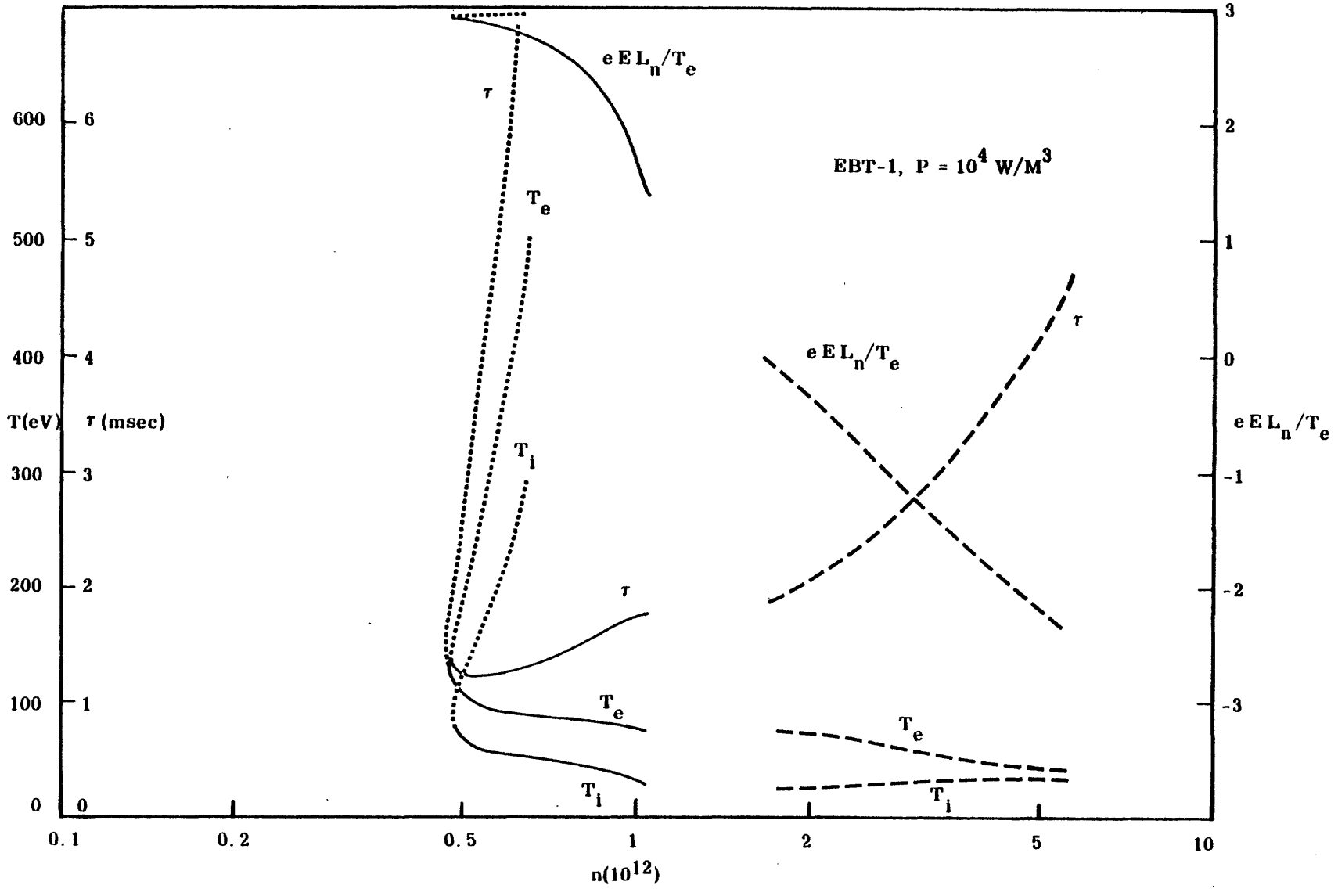

FIG. 5. Operating characteristics for EBT-I.